Preparation and characterization of poly(ethylene terephthalate) films coated by chitosan and vermiculite nanoclay

Fatima Essabti[a], Alain Guinault[a], Sébastien Roland[a], Gilles Régnier[a], Saïd Ettaqi[b], Matthieu Gervais[a,*]

[a] PIMM, Arts et Métiers ParisTech, CNRS, CNAM, 151 Bd de l'Hôpital, 75013 Paris, France
[b] Laboratory Materials, Metallurgy and Process Engineering, ENSAM, Meknes, Morocco

Keywords:
Chitosan
Vermiculite
Poly(ethylene terephthalate)
Barrier properties
Food packaging
Coating

A B S T R A C T

Chitosan (CS) layers are coated on a poly(ethylene terephthalate) (PET) film in order to decrease the oxygen permeability through the polymeric films for food packaging applications. Oxygen transmission rate (OTR) of the 130 µm PET films can be decreased from 11 to only 0.31 cm^3/m^2.day with a coated layer of 2 µm of CS. Additional decrease is obtained with the addition of vermiculite (VMT) to CS matrix in high proportion (40 to 50 w/w%). The OTR of the coated PET films decreased to very low values, below the detection limit of commercial instrumentation (≤ 0.008 cm^3/m^2 day). This high-barrier behavior is believed to be due to the brick wall nanostructure, which produces an extremely tortuous path for oxygen molecules.

1. Introduction

Plastics have been widely adopted in food packaging because of their advantages over other materials. These advantages are reflected in the physical, mechanical and chemical properties of plastics (Rhim, Park, & Ha, 2013; Tharanathan, 2003). Nevertheless, the environmental impact of persistent plastic packaging wastes is raising general global concern, since disposal approaches are restricted (Wikström, Williams, & Venkatesh, 2016). The increasing environmental pollution makes research on the development of packaging from renewable resources essential (Chung et al., 2010; Fajardo et al., 2010; Tharanathan, 2003). Nowadays, food safety and environmental concerns have forced food industry to design safer and eco-friendlier packaging. Edible films and coating based on natural biopolymers such as polysaccharides have received increased attention as an alternative to synthetic food packaging due to their biodegradable and edible properties as well as their use as active packaging (Bourtoom, 2008; Dehghani, Hosseini, & Regenstein, 2018). For example poly(ethylene terephthalate) (PET) films coated with poly(vinylidene chloride) (PVDC) (Haworth & Robinson, 1991) are industrially used for food packaging applications while they induce a waste problem as their incineration creates toxic products (increases the amount of dioxins formed in the incinerator of household wastes due to the presence of the chlorine in PVDC) (Bhaskar, Tanabe, Muto, & Sakata, 2006; Liu et al., 2015; Ohta et al., 2001; Ohta, Oshima, Osawa, Iwasa, & Nakamura, 2004). To avoid this, the use of biopolymers is proposed as a coating alternative (Roilo, Maestri, Scarpa, Bettotti, & Checchetto, 2018; Tharanathan, 2003). CS is one of a few natural polysaccharide that may be a solution to the environmental problem (Fajardo et al., 2010; Tharanathan, 2003) for food packaging films (Dehghani et al., 2018; Shahidi, Arachchi, & Jeon, 1999). Furthermore, CS films have good oxygen-barrier properties in dry conditions due to the huge quantity of hydrogen bonds in the polymer, comparable to many commercial synthetic polymers (Caner, Vergano, & Wiles, 1998; Epure, Griffon, Pollet, & Avérous, 2011; Madeleine-Perdrillat et al., 2015; Sánchez-González, Cháfer, Chiralt, & González-Martínez, 2010). Despite those attractive properties, there are limitations for the use of pure CS, as its natural hydrophilicity and the insufficiency of its water vapor barrier properties limit its use for packaging applications (Lertsutthiwong, Noomun, Khunthon, & Limpanart, 2012; Lewandowska, Sionkowska, Kaczmarek, & Furtos, 2014; Reis, Yoshida, Reis, & Franco, 2011). Indeed, it is sensitive to moisture because of its capacity to form a large number of hydrogen bonds. This is due to the presence of three different polar functional groups, namely, hydroxyl (OH), primary amine (NH_2), and ether (C-O-C) groups, also depending on the deacetylation level residual carbonyl (C═O) groups (Elsabee & Abdou, 2013; Madeleine-Perdrillat et al., 2015). Various approaches have been taken into consideration to improve the barrier properties of the CS film, such as blending with the other biodegradable polymers (Abugoch, Tapia, Villamán, Yazdani-Pedram, & Díaz-Dosque, 2011; Benbettaïeb, Karbowiak, Bornaz, &

* Corresponding author.
E-mail address: matthieu.gervais@lecnam.net (M. Gervais).

Debeaufort, 2015; Kurek, Galus, & Debeaufort, 2014; Ren, Yan, Zhou, Tong, & Su, 2017), high-energy irradiation (Benbettaïeb, Assifaoui, Karbowiak, Debeaufort, & Chambin, 2016; Benbettaïeb, Karbowiak, Brachais, & Debeaufort, 2015), crosslinking by a chemical agent (Yu, Song, Shi, Xu, & Bin, 2011) and the most recent method is based on incorporating a nanoscale filler (Casariego et al., 2009; Lertsutthiwong et al., 2012; Tang et al., 2009; Wang, Shen & Tong et al., 2005; Yixiang, Xi, & & A, 2006). The field of nanocomposites reinforced with clay have gained considerable academic and industrial attention, because of their possibilities to improve mechanical and barrier properties of films (Rhim et al., 2013; Sinha Ray & Okamoto, 2003). In recent years, nanoclays have been widely studied as an additive to reduce the gas permeability of various biodegradable polymers (de Azeredo, 2009; Bordes, Pollet, & Avérous, 2009; Rhim et al., 2013; Tang et al., 2009; Wang, Shen & Tong et al., 2005; Xu, Ren, & Hanna, 2006). Recent investigations have shown that the incorporation of inorganic nanoparticles such as clay into CS is greatly effective in enhancing physico-mechanical properties while many useful properties such as improved gas barrier properties and retained transparency are simultaneously achieved (Laufer, Kirkland, Cain, & Grunlan, 2013; Wang, Shen, Zhang, & Tong, 2005). To the best of our knowledge, very few studies have addressed the preparation of CS nanocomposites based on VMT nanoclays for food packaging applications and particularly with high content. The introduction of impermeable fillers into materials makes it possible to increase the barrier properties but their effect is marked definitely more if they have a high aspect ratio which extends the diffusion pathway of the molecules (increase in tortuosity) (Sinha Ray & Okamoto, 2003). For this reason, VMT was chosen as it exhibits a high aspect ratio. The size of the exfoliated VMT particles is generally in the range of 0.5–16 mm. Fillers are generally added in a few weight percent due to the difficulty to introduce the fillers through melting with a great increase in viscosity. Low content of fillers leads generally to a decrease by a factor 3 to 4 of the gas permeability. Higher filler content, achieved in solution, is known to address better results and the use of filler content up to 50 wt% can lead to a high decrease in gas permeability (factor from 10 to 100) (Giannakas, Spanos, Kourkoumelis, Vaimakis, & Ladavos, 2008; Gorrasi et al., n.d.; Picard, Vermogen, Gérard, & Espuche, 2007; Rhim, 2011; Takahashi et al., 2006; Tortora et al., 2002; Wang & Jing, 2017). The main challenge for preparing nanocomposites is the nanoscale dispersion of clay in the biopolymer matrix (microcomposites, intercalated nanocomposites or exfoliated nanocomposites). The nano-filler incorporation into the polymer matrix can be carried out with three main techniques (Ray & Bousmina, 2005; Sinha Ray & Okamoto, 2003): the in-situ polymerization, the melt intercalation process or the solvent intercalation. This last elaboration process is based on a solvent system in which the polymer is soluble and the silicate layers are swellable. The polymer is first dissolved in a solvent. In parallel, the clay (modified or not) is swollen and dispersed into the same solvent or another one to obtain a miscible solution. Both systems are pooled together leading to a polymer chain intercalation. Then, the solvent is evaporated to obtain nanocomposite materials. It is this latter method which was selected for this study. This technique was used because CS cannot be melt processed due to high thermal and thermomechanical degradations. In recent years, layered materials have also received considerable attention because of their advantages over synthetic films (Bourtoom, 2008; Dehghani et al., 2018).

However, a few studies have been conducted on the influence of processing on the gas permeability properties and structural stability of chitosan coated PET films especially with nanoloads (Laufer et al., 2013). The aim of the current work was to study the coating of PET films with CS using an industrially available process leading to thin layers (~ 1 µm) in the first step and then with nanocomposites based on CS-VMT in the second step. Effects of fillers content exceeding 5% contrary to most of the literature up to values of 25, 40, and 50 wt% on helium and oxygen gas barrier properties of the films were studied.

2. Material and methods

2.1. Materials and reagent

VMT water dispersion (MicroLite 963 - dry content 9 wt. %) used in this work was supplied by Specialty Vermiculite Corp Company, Canada. Granulometry varies in the range of 0.5 mm–15 mm and % OSP (Over Sized Particles refers to the percentage of particles retained on a 45 µm screen) was ≤ 8%. CS was obtained from the shrimp shell by Glentham Life Sciences (Wiltshire, United Kingdom), ($\overline{M_w}$ = 890 000 kDa; viscosity: 0.1–0.3 Pa.s and degree of deacetylation > 95%). Distilled water and acetic acid (glacial 100%, Merck, Darmstadt, Germany) were used as received. A commercial 130 µm poly(ethylene terephthalate) (PET) film was coated respectively with CS solution and CS-VMT solutions. A commercial Toray 12 µm thick PET film coated with a 2 µm Solvay IXAN-DIOFAN PVDC layer was used as received. No further purification of chemicals has been realized and freshly prepared solutions were always used.

2.2. Film preparation

2.2.1. Preparation of chitosan and nanocomposite solution

CS solutions were prepared by dissolving 1 g of CS in 50 mL of 1% (v/v) aqueous acetic acid solution and stirred continuously overnight at room temperature to obtain homogenous mixture. For nanocomposites solutions, an amount of inorganic cations VMT crystals dispersed in water (9 wt%) was diluted in the same solvent as CS. The volume of water dispersion and aqueous acetic acid dilution varies with the expected final composition of VMT (details presented in Table 1). The resulting slurry was kept stirring for 24 h at room temperature. Finally, CS-VMT nanocomposites solutions were prepared by gradually adding diluted VMT into the CS solution at room temperature, and then the resulting mixture was stirred for another 24 h using magnetic stirrer.

2.2.2. Chitosan/nanocomposite coated PET films

Aqueous solutions could not be coated correctly on PET film due to polarity differences. To improve the wetting of the film, prior to deposing aqueous solution of CS/nanocomposite, PET films were corona treated with a mini corona treater (from Electro Technic Products Society (Chicago, USA). PET films were cut approximately about 12.5 cm in width and 23.0 cm in length and cleaned with ethanol. PET film is guided via a roller at different speeds below the electrode installed at a height of 0.5 cm and constant voltage (40 kV). Several films were prepared in order to optimize the exposure time of the corona treatment. This last was calculated as follows (Eq. (1)):

$$Exposure\ time = \frac{distance}{speed} \quad (1)$$

Where distance equal to 0.125 m and speed varied from 0.5×10^{-3} to 2.2×10^{-2} m s^{-1}.

The layered films were prepared by a bar-coating technique: aqueous acetic acid 1 wt% solutions of CS or CS-VMT nanocomposites were

Table 1
Compositions and dry extracts of the various coatings.

V_{CS} initial (mL) ([CS] = 20 g/L)	$V_{initial}$ (VMT solution) (dry content 9 wt%) (mL)	$V_{(H2O/Ac\ acid\ 1\%(v/v))}$ added to VMT (mL)	$[VMT]_{obtained}$ (g/mL)	CS/VMT solution dry extract (g/mL)	Final wt% VMT
50	4.5	9.9	0.33	1.26	25%
50	8.0	19.8	0.60	1.20	40%
50	12.0	30.0	1.00	1.16	50%

coated with a 50 µm barcoater on 130 µm corona-treated PET films. This coating has been repeated up to three times with a drying step under vacuum at 45 °C for 15 min between each coating and dried under the same conditions for 12 h at least at the last step.

2.3. Characterization methods

2.3.1. Surface energy determination

The surface tension of films (γ_s) and its polar (γ_{ps}) and dispersive (γ_{ds}) components were determined using the (Owens & Wendt, 2003) method (Eq. (2)).

$$\gamma_l(1 + \cos\theta) = 2(\gamma_{ds}\gamma_{dl})^{0.5} + 2(\gamma_{ps}\gamma_{pl})^{0.5} \quad (2)$$

Where θ, γ_l, γ_{dl} and γ_{pl} are respectively the contact angle, the surface tension, the dispersive and the polar components of the tested liquid; γ_{ps} and γ_{ds} are the polar and dispersive components of the tested surface. The contact angle measurements were carried out using the sessile drop method on a goniometer (GBX, France) equipped with image analysis software. A drop of the tested liquid was placed on the surface of the totally smooth horizontal film, using four liquids of different polarities: water (solvent used to prepare the coating solution), ethylene glycol-H_2O 10%, glycerol, and diiodomethane. According to (Ström, Fredriksson, & Stenius, 1987) and (Fowkes, 1964), liquid polar contributions (γ_{pl}) were 51.0, 16.8, 26.4, and 0 mN m^{-1}, while their corresponding dispersive contributions (γ_{dl}) were 21.8, 30.9, 37.0, and 50.8 mN m^{-1}, respectively.

2.3.2. Dynamic light scattering method (DLS) measurements

Solutions of VMT (1 g) were prepared at different quantities of aqueous acetic acid 1 wt%, varying from 20, 30, and 50 ml. After 48 h of stirring, these solutions were characterized by DLS method. Dynamic Light Scattering (DLS) measurements were performed on Malvern ZetaSizer ZEN3600 instrument (UK) equipped with a 633 nm laser (scattering angle 175°) at 25 °C. DLS technique primarily measures time-dependent fluctuations of scattered coherent light, i.e. the decay of the autocorrelation function, which is caused by diffusive motion of the particles. The average diffusion coefficient (D) of the particles in solution can be used to obtain the hydrodynamic diameter, D_h, via the Stokes–Einstein Eq. (3), as follows (Berne & Pecora, 2000):

$$D = \frac{k_B T}{D_h 3\pi\eta_0} \quad (3)$$

Where k_B is the Boltzman's constant, η_0 is the viscosity of the solvent and T the temperature.

2.3.3. Atomic force microscopy (AFM)

After corona treatment, the surface topography and the films roughness were analyzed with AFM. Tapping mode images were obtained by using a Multimode microscope driven by a Nanoscope V controller (Veeco, USA) and operated under atmospheric conditions. The tips (silicon, spring constant 40 N/m, oscillation frequency ca. 300 kHz) were supplied by BudgetSensors. The tips have a curvature radius below 10 nm. Images of 1 µm^2 surface scans were recorded in tapping mode with a silicon cantilever to avoid the effect of interaction with the sample surface. NanoScope Analysis software was used to obtain roughness parameters values after a plane fit procedure. Roughness value is the arithmetic average obtained as follow, Eq. (4):

$$R_a\,(nm) = \frac{1}{n}\sum_{i=1}^{n} |y_i| \quad (4)$$

Where y_i is the vertical distance from the mean line. This average value is obtained over an entire AFM image.

2.3.4. Scanning Electron Microscopy (SEM): observation and thickness analysis

In order to evaluate the coating thickness (PET/1 layer, PET/2 layers, and PET/3 layers), coated films were prepared using an ultramicrotome (LKB BROMMA 2088 - ULTROTOME V, Sweden), equipped a diamond knife at ambient temperature. Then, the film thickness of each layer was estimated using SEM (Hitachi 4800 SEM). The thicknesses were observed using an accelerating voltage of 0.7 KV. The thicknesses reported are the average value of at least 8 measurements performed at different points of the film.

2.3.5. Transmission electron microscopy (TEM)

Samples of CS-VMT were prepared by casting. The cast films were then sectioned perpendicular to their surface with an ultra-microtome 2088 Ultrotome V (LKB, Sweden) equipped with a diamond knife at a cutting rate of 1 mm/s. Thin slices of 70–80 nm were collected on 300 mesh square copper grids and subsequently dried with filter paper for observation. The TEM microscope is a CEM 902 Zeiss microscope (Germany) operating under a voltage acceleration of 80 kV equipped with a Camera Digitale ProgRes MFscan. Images of 2.5 µm^2 were collected from different slices for each film.

2.3.6. X-ray diffraction

WAXS measurements of the chitosan and nanocomposite films were performed on the high brilliance SWING beam line at the Soleil Synchrotron facility, with a monochromator set at 16 keV (David & Pérez, 2009). Using a CCD detector at 0.5 m from the sample, diffraction patterns were recorded for reciprocal spacing $q = 4\pi\sin(\theta)/\lambda$ varying between 0.20 and 2.74 Å where 2θ is the scattering angle and $\lambda = 1.03$ Å is the X-ray wavelength.

By using Foxtrot software, 1D WAXS curves were obtained by circular averaging of the full 2D images (0–360°). 10 images were recorded for each sample and 1D curves were averaged in order to obtain 1 curve for each sample.

The basal spacing (d_{001}) value of the layered silicates films were computed using Bragg's equation (5):

$$\lambda = 2d_{001}\sin\theta \quad (5)$$

2.3.7. Helium and oxygen permeability

The helium permeance was measured at 23 °C and 0% relative humidity (RH), by a specific home-made analyzer, based on the ISO 15105-2:2003 method. Circular portions cut from the films (surface = 23.75 cm^2) were inserted between two hermetically sealed compartments drained using nitrogen. A helium constant flow (80 mL min^{-1}) was introduced in the downstream part of the cell and is measured in the upstream part, using a helium detector (mass spectrometer ADIXEN 142 (France)). The OTR (oxygen transmission rate) was measured with a Systech analyzer 8001 (United Kingdom) at 23 °C and 0% RH on film samples. Oxygen permeance was obtained by multiplying respectively the OTR by the pressure (1 bar). Barrier improvement Factor (BiF) is defined as the ratio between the permeance of the coated film and the permeance of the uncoated PET film.

Then, the permeability of the coated layer was calculated using Eq. (6).

$$\frac{1}{P_{PETC}} = \frac{th_{PET}}{th_{PETC}}\frac{1}{P_{PET}} + \frac{th_{CL}}{th_{composite}}\frac{1}{P_{CL}} \quad (6)$$

Where P_{PETC} is the permeability of coated PET, th_{PETC} the thickness of coated PET, P_{CL} the permeability of coated layer, th_{CL} the thickness of coated layer, P_{PET} the permeability of PET film and th_{PET} the thickness of PET film. The tests were repeated three times for oxygen permeability and five times for helium permeability with film change after each test.

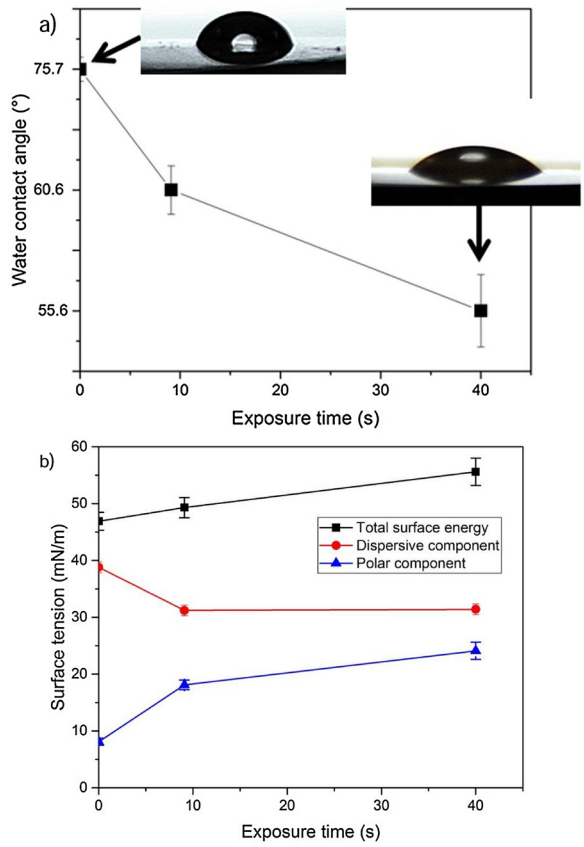

Fig. 1. a) Water contact angle on PET films versus exposure time b) Variation in total surface energy and dispersive and polar components of PET film as a function of exposure time.

3. Results and discussion

3.1. Chitosan coated PET films

3.1.1. Effect of the corona treatment on the PET films surface

The water contact angle of an untreated PET film is 75.7°. It decreased after 10 s Corona treatments to 60.6° and after 40 s to 55.6° (Fig. 1a). The variation in the surface energy of the PET surfaces as a function of the corona exposure time is illustrated in Fig. 1b. Results show a clear increase in the value of the calculated surface energies of PET after corona treatment. The total surface energy is increased up to 55.6 mN m^{-1}, in comparison with the total surface energy of PET which has a value of 46.9 mN m^{-1}. The increase in total surface energy is due to the strong increase in the polar component of the surface energy which is due to the incorporation of oxygen and nitrogen on the surface of the polymer as alcohol, amine or carboxylic acid functions (Sutherland, Popat, Brewis, & Calder, 1994). This is the interesting component as a strong polar solvent (water) is used for the coating step. The dispersive component is decreased with the treatment.

The reduction in the contact angles mentioned previously is reflected by an increase in the surface energy of the PET after the corona treatment its results in an increased wettability of the solvent used. This increase is due to a clear increase in the polar component despite a decrease in the dispersive component. If the surface tension is affected, it is due to the chemical functions on the surface that has been modified during the treatment. It is mainly due to the formation of polar groups such as CO, COO, OH, etc. (O'Hare et al., 2002; Pochan, Gerenser, & Elman, 1986). These results are in good agreement with those reported in literature (Tsay & Pai, 2018), showing an increase in the polar contribution as a main consequence of polar groups formation induced by plasma/corona treatments. Low-density polyethylene samples

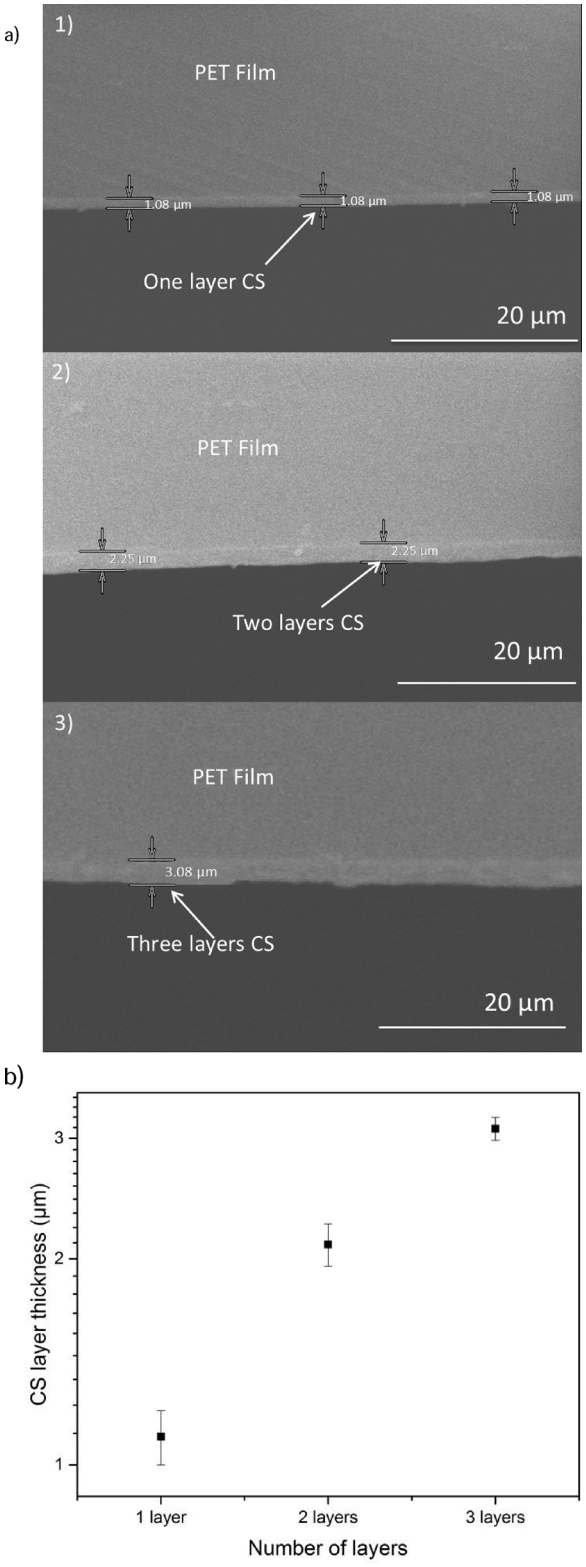

Fig. 2. a) SEM cross-section micrographs thickness pictures of the PET films with coated layers: 1) one layer chitosan, 2) two layers chitosan and 3) three layers chitosan b) Average thickness of coated layers measured by SEM.

functionalized by corona treatment was used also (Park & Jin, 2001), confirming that the corona treatment under air causes the oxidation of the surface.

The surface morphology and roughness of both the untreated and the corona treated PET film were analyzed using atomic force

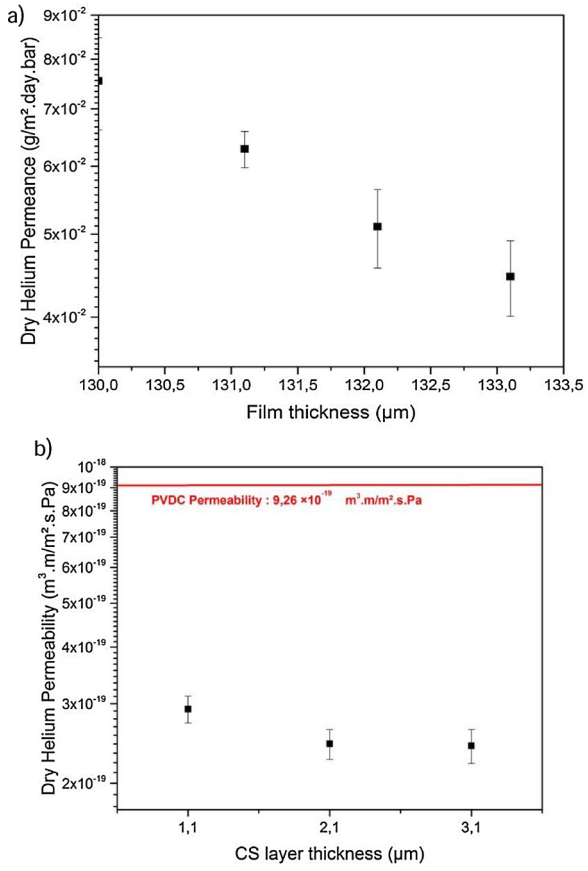

Fig. 3. Helium permeance CS coated PET films (a) and helium permeability of coated CS layers (b) both in dry condition (23 °C and 0% RH).

microscope (AFM) (Data not shown). AFM images illustrate that the surface of untreated PET film surface was relatively smooth with protuberances and moderate roughness. After the corona treatment, the size of the protuberances has increased with increase in exposure times. It is seen that the values of roughness gradually increase with increasing exposure time. The roughness is increased due to the removal of top few monolayers of the polymer films, caused by the impact of electric discharge of corona on the surface, going from a R_a value of 1.35 nm without treatment to 3.99 nm with an exposure time of 40 s to corona treatment which is similar to those reported in literature (Han, Kim, & Park, 2014; Rocca-Smith et al., 2016). Following the theory of adhesion (Shenton & Stevens, 2001), this roughness could act positively on the coating adhesion by creating much more specific surface. It is classically observed with the corona treatment.

3.1.2. Microstructure and thicknesses

After having optimized the corona treatment, coatings on corona treated PET films were performed. Cross-section micrographs of CS coated PET film observed by SEM (Fig. 2a) show the absence of pores or other inclusion that could occur when air bubbles are present in the casting solution. SEM images show continuous uniform layers without apparent defects, exhibiting good adhesion between the PET film and layers of CS. Indeed, no voids are present between the PET film and the coating, clearly assessing the good coating adhesion. The total thicknesses of coated films were estimated using SEM. The measurement of the coating thickness is particularly important for several reasons; the most important is that gas barrier properties are strongly dependent of the layer thickness (Haworth & Robinson, 1991). Thus, it is important to verify that the thickness of the coated layers is as homogeneous as possible so the phenomena of transfer will be identical in any point of the section of the film. The thickness of the coated layers varied between 1.1 µm for one layer to 3.1 µm for 3 CS layers (Fig. 2b).

3.1.3. Helium barrier properties of chitosan-coated PET films

The results of measurements of the helium permeance of the CS coated PET films are represented in Fig. 3a. The coated films were significantly less permeable than the uncoated one. This decrease was undoubtedly attributed to the presence of the thin CS layer. A linear decrease of the Helium permeance of the film is observed with the increase of the thickness of the coating from 0 to around 3 µm. In order to understand the behavior of the CS, the permeability of the CS layer is calculated from Eq. 4 and is shown in Fig. 3b. A decrease of permeability of CS is observed from 1 to 2 µm and then this value stays stable at 3 µm. This decrease is however quite negligible with the error made on the thickness of the layer and the evolution is in the range of the error bars. In the present work, the value of helium permeability for CS film is measured as 2.4×10^{-19} m^3 m/m^2 s Pa with a layer thickness of 2.1 µm. This value is comparable with those of existing commercial synthetic films such as PVDC 9.4×10^{-19} m^3 m/m^2 s Pa (measured on the same apparatus).

3.2. Nanocomposite CS-VMT coated PET films

3.2.1. Vermiculite dispersion in acetic acid/water solutions

Recently, intercalation of clay in several polymers has been introduced as a promising route, leading to versatile polymer composites, especially those containing a nanoscale silicate of high aspect ratio. Because of the small size of the structural unit and the high surface-to-volume ratio, the properties of nanocomposites are greatly influenced by the degree of mixing between the two phases (Azeez, Rhee, Park, & Hui, 2013; Pavlidou & Papaspyrides, 2008). In this work, we build a better barrier by adding VMT to CS matrix. DLS characterization is an interesting technic to observe the dispersion of the VMT in acetic acid/water solutions. Two peaks are detected, for 1 g of VMT dispersed in 20 ml acetic acid/water 1% v/v, showing VMT with size of 1 and 10 µm. In contrast, a single peak is observed for 1 g of vermiculite dispersing in 30 and 50 mL of acetic acid/water 1% v/v. This suggests that no aggregate is observed for a concentration equal or lower than 33 g/L and that the observed size is of 1 µm. Therefore, a concentration of 30 g/L in

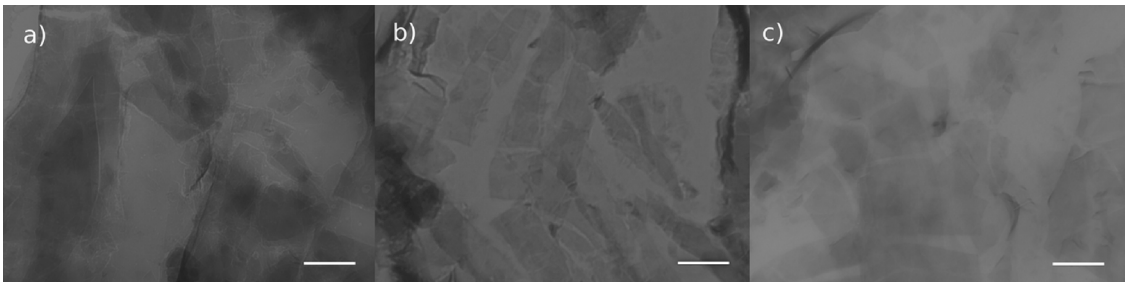

Fig. 4. TEM micrographs of thin sections, viewed at 80 kV, of the cast films CS-VMT: a) CS-25%VMT, b) CS-40%VMT c) CS-50%VMT (the scale of the images is 250 nm represented in white line).

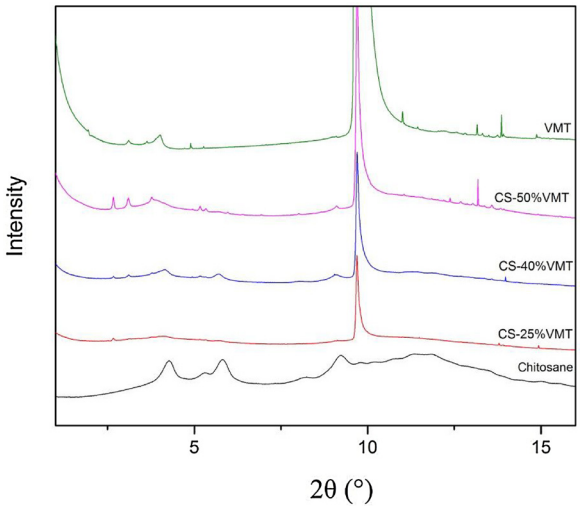

Fig. 5. XRD patterns of pure VMT, neat CS, CS-25%VMT, CS-40%VMT, and CS-50%VMT.

VMT has been the highest concentration used in the following experiments to avoid any aggregation. To verify that no aggregation is observed after mixing VMT with chitosan and drying of the solution, TEM images of casted solutions have been realized. Fig. 4(a–c) displays the TEM microtomed cross section of cast films of CS-VMT containing CS-25%VMT, CS-40%VMT and CS-50%VMT nanocomposite showing the presence of exfoliated VMT within the CS matrix. The hydroxyl groups in chitosan can form hydrogen bonds with the hydroxyl groups of the acid-modified VMT surface, and this interaction existing between chitosan and acid-modified VMT surface by comparing TEM images. These images show that there is no aggregation in the CS-VMT solution due to the mixing of the two solutions. The nanosheets disorderly dispersed within the chitosan matrix with a high width to-thickness ratio.

The clay dispersion within chitosan has also been characterized by XRD. Fig. 5 shows the XRD patterns of pure VMT, neat CS, and CS/MMT nanocomposites with different VMT concentrations. The XRD pattern of neat CS shows the characteristic crystalline peaks at 2θ of 4.18°, 5.73° and 9.13°. These crystalline peaks become less intense after incorporating VMT into chitosan. This result is consistent with (Wang, Shen & Zhang et al., 2005). In this study the researchers showed that the crystallinity of chitosan increases after the addition of MMT up to a level of 5%, followed by the decrease of crystallinity when proportion of MMT increases to 10%. This may explain the flattening of the peaks of crystalline phase of chitosan since higher rates of VMT were added in our study. Besides, the XRD pattern of the VMT shows a reflection peak at 2θ of 9.65° corresponding to a basal spacing of 6.1 Å calculated using Bragg's equation. This characteristic peak of the clay decreases in the XRD spectra after incorporating CS within VMT but remains present. This indicates that the layered clay is not fully delaminated in the chitosan/VMT film. However the appearance of peaks at 2.65° and 3.08°, corresponding to 22.4 and 19.8 Å respectively, indicates that an intercalated structure composed of CS within the VMT layers is obtained which increases the basal spacing of VMT as already reported in literature (Petrova et al., 2012).

Fig. 6 presents the images of PET films coated with two layers of CS-VMT with various rates of VMT. The transparency of edible/bio-based polymer films is a key parameter to good film acceptance by users (Rhim, Gennadios, Weller, & Hanna, 2002). First of all, visually all the showed films were transparent, for either uncoated PET or PET coated with CS (Fig. 6a, b). Also, it can be noticed that nanocomposites films had a translucent surface (Fig. 6c–e). The brightness of all films

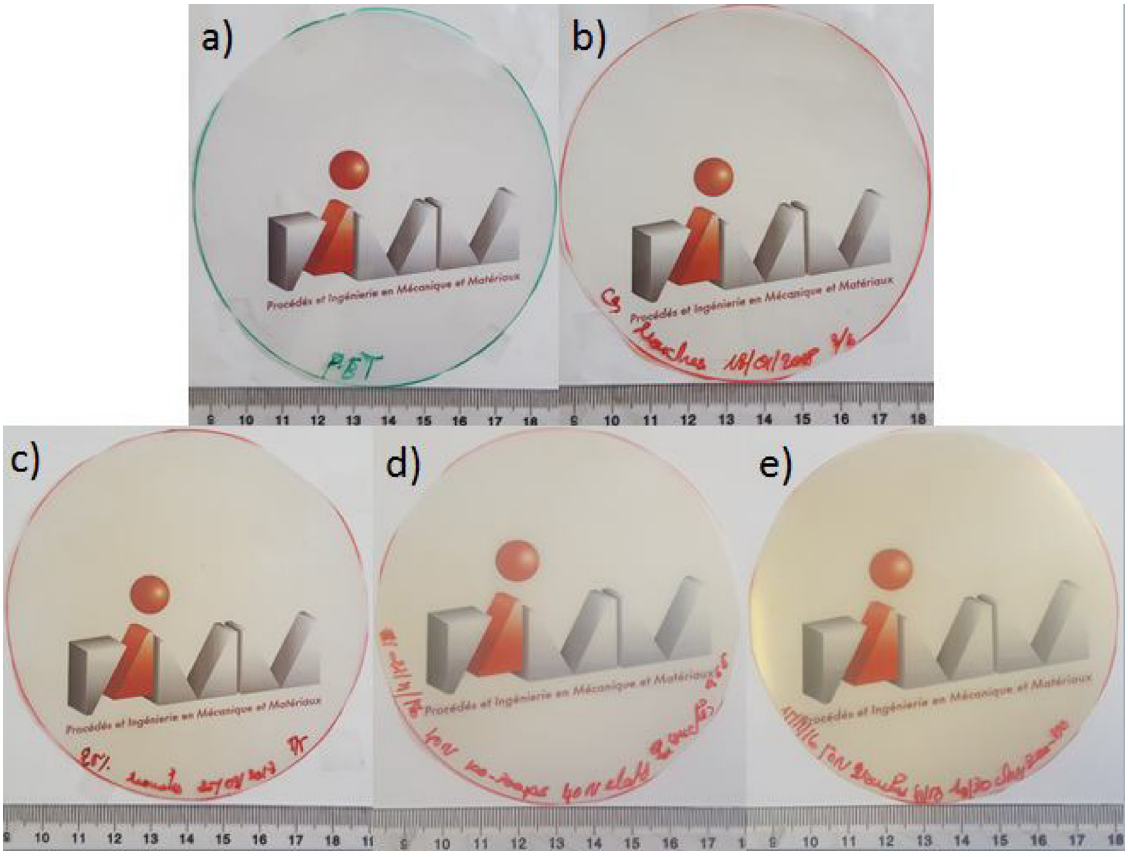

Fig. 6. Images of films coated with two layers : a) uncoated PET b) PET coated with CS c) PET coated with CS-25%VMT d) PET coated with CS-40%VMT e) PET coated with CS-50%VMT.

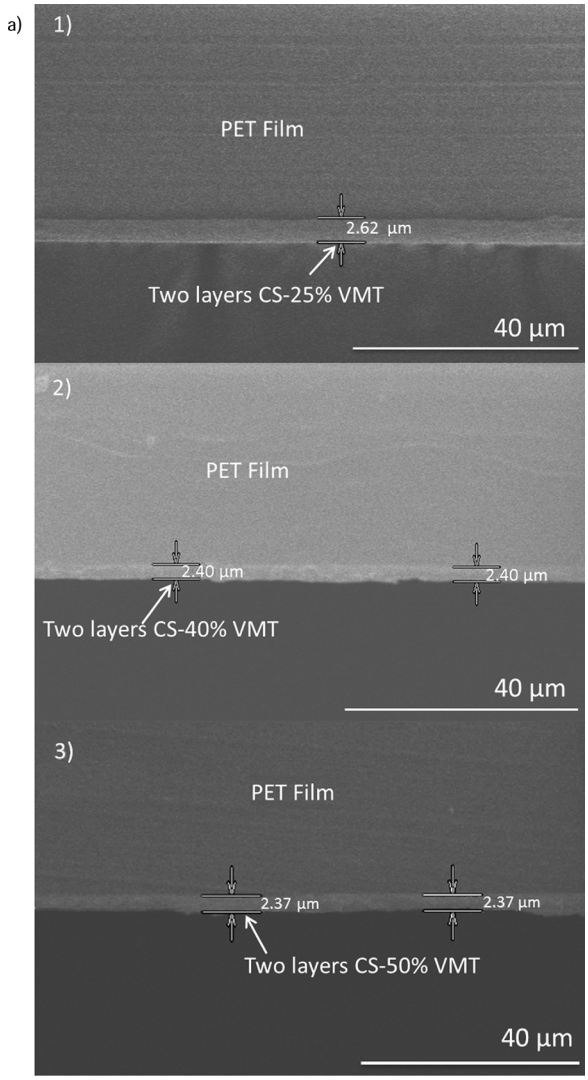

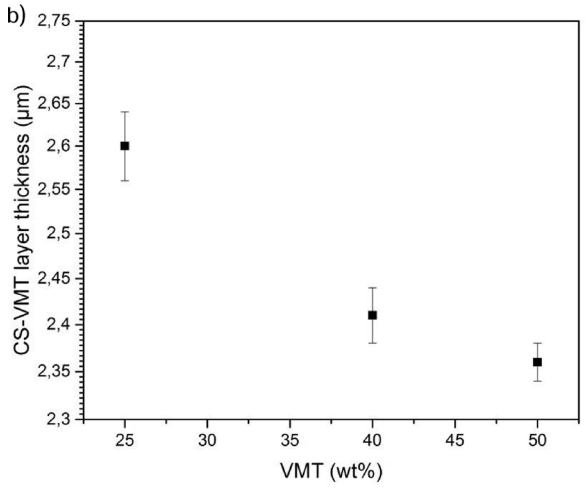

Fig. 7. a) SEM cross-section micrographs thickness pictures of the PET films with coated layers: 1) two layers CS-25%VMT, 2) two layers CS-40%VM and 3) CS-50%VM. b) Average thickness of two layers CS-VMT coated PET film measured by SEM.

remained fairly constant, for VMT percentage varying from 0 to 25%. However, the presence of 40, 50, and 60% of VMT in the coated films increases significantly the yellow tint. To conclude, all the films were visually noticeable, and thus they could be used as edible films or coatings.

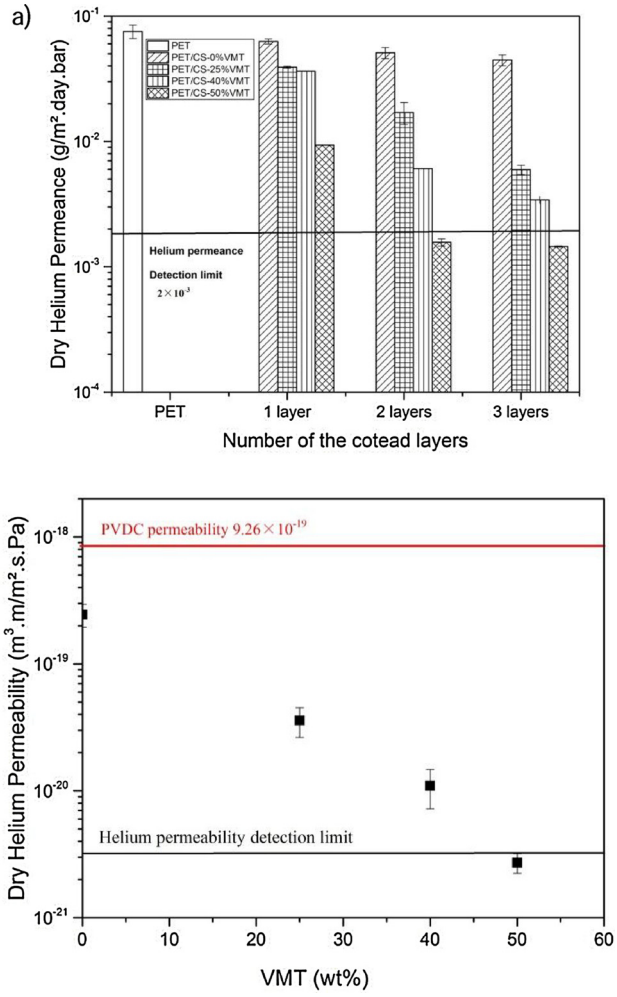

Fig. 8. Helium permeance of a PET film coated with two layers of CS-VMT (a) and helium permeability of two coated layers of CS-VMT (b) both in dry condition (23 °C and 0% RH).

3.2.2. Microstructure and thicknesses of nanocomposite CS-VMT coated PET

In this part, the system with two coated layers is only used for nanocomposite aspect as it should lead to a 2 µm thick layer which corresponds to classical PVDC industrial coatings. Thicknesses of CS/VMT coated layers were measured in the same way as reported with the single layered chitosan-coated PET films. Fig. 7a shows the SEM images of PET films coated with different amounts of nanofillers. These images show continuous and uniform layers without apparent defects, exhibiting good adhesion between the PET film and layers of CS-VMT like CS coated PET films. We can conclude that the presence of VMT does not alter the formation of these layers. In addition, Fig. 7b shows the little decreasing of the thickness of the coated two layers of CS-VMT with increasing the nanofiller rate, perhaps due to a lower solubilization of the first layer when applying the second one in comparison to unfilled layer. The thickness varied from 2.60 to 2.36 µm for respectively 25% and 50% of VMT.

3.2.3. Helium barrier properties of chitosan/vermiculite coated PET films

As showed before, the permeability of PET films seems to be unvaried after the deposition of more than two layers of CS indicating that there is no need for an additional layer to obtain a stable behavior. So, for the following experiments, PET films coated with two layers of CS-

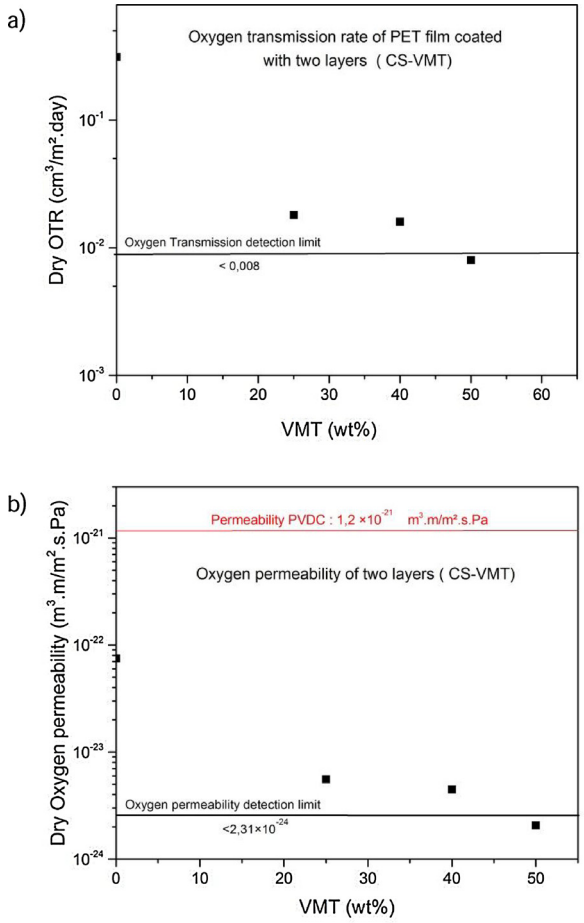

Fig. 9. Oxygen transmission rate of a PET film coated with two layers of CS-VMT (a) and oxygen permeability of two coated layers of CS-%VMT (b) both in dry condition (23 °C and 0% RH).

VMT will be studied. The results of measurements of the helium permeance of the PET films according to the coated layers with CS-VMT are represented in Fig. 8a. The coated films with CS-VMT are significantly less permeable than the uncoated PET film. The presence of VMT in the chitosan layers decreases the helium permeance of coated PET films. Firstly, a decrease in the permeance of the nanocomposite coated films is observed when the number of coated layers increases; this result is in good agreement with the previous ones. Also, it is accompanied with a decrease of permeance when the composition of the nanocomposite is increased in VMT. BiF of around 100 was obtained when adding 50% of vermiculite. It should be noted that even higher effect on the gas barrier properties could be expected, however, the limit of detection of the apparatus is attained and the evolution cannot be detected as seen in Fig. 8a, as well as the permeance becomes nearly stable from two layers on nanocomposite from 50% VMT fillers. From a kinetic point of view, the gas permeation is much faster for a layer and it results in a higher gas permeance. This is explained by the decrease in the permeance of the CS/VMT when the thickness of the coated layer increases. These results lead to calculate the helium permeability of coated layers (Eq. (4)). Helium permeability of two layers of nanocomposite versus the VMT fraction of the nanocomposite is presented in Fig. 8b. In the present work the helium permeability decreases after adding VMT fraction to the CS, also when the composition of the nanocomposite increased on VMT. It can be noted that the helium permeability of two layers of nanocomposite decreases from 24.4×10^{-20} (m^3.m/m^2.s.Pa) up to 1.1×10^{-20} (m^3 m/m^2 s Pa) by only adding 40% of vermiculite to chitosan in dry conditions. Even higher effect on the gas barrier properties could be expected for 50 and 60 wt. % vermiculite, as said previously.

3.3. Oxygen transmission rate of chitosan and chitosan/vermiculite coated PET films

The presence of oxygen in the packaged foods can cause many deteriorative reactions such as nutrient losses, color changes, off-flavor development, and microbial growth. It has also a considerable effect on the respiration rate and ethylene production in fruits and vegetables (Elsabee & Abdou, 2013). For these reasons, limited oxygen migration within food packaging is desirable. Fig. 8a shows the OTR results of PET films coated with two layers of CS and CS-VMT. These results allowed us to calculate the permeability of coated layers (Eq. 4) (Fig. 9b). As we can observe in Fig. 9a alone CS brings a clear improvement of the OTR, this value decreases from 10.9 to 0.3 cm^3/m^2 day. In the present work, the oxygen permeability of CS is 7.5×10^{-23} m^3 m/m^2 s Pa. This value is lower than commercial synthetic films of PVDC (1.2×10^{-21} m^3 m/m^2 s Pa). Also, this value is lower than those reported in literature (8×10^{-21} (Duncan, 2011; Kurek, Guinault, Voilley, Galić, & Debeaufort, 2014; Sathivel, Liu, Huang, & Prinyawiwatkul, 2007)), (1.65×10^{-19}(Kurek & Galus et al., 2014)), (6.79×10^{-18} (Cussler, Hughes, Ward, & Aris, 1988)), (3.13×10^{-16} (Kurek et al., 2013)), (1.77×10^{-14} (Kurek, Ščetar, Voilley, Galić, & Debeaufort, 2012). A lower value is observed in this study which might be explained by the difference in the fabrication process used and by the final total thickness of the chitosan layer that are very thin compared to what was presented by the other authors. A better drying of the layer is expected compared to the ones observed in literature as this layer is thinner. With thicker ones, water should not be able to be completely extracted properly from the core of the layer as soon as a superficial layer of chitosan is dried up meaning a non-negligible amount of water is in the layer. The used drying process is also longer with relatively low temperature (45 °C) and is under vacuum. According to results presented in Fig. 9(a,b) it can be noticed that the OTR of the PET coated films decreases from 3.12×10^{-1} to 1.6×10^{-2} cm^3/m^2.day by only adding 40% of VMT to CS in dry conditions. Also, PET film coated with 50% of VMT, where coating is 2.36 μm thick, exhibits an OTR below the detection limit of commercial instrumentation ($\leq$ 0.008 cm^3/m^2 day). Oxygen permeability decreases after adding VMT fraction to the CS, also when the composition of the nanocomposite increased on VMT. It can be noted that the oxygen permeability of two layers of nanocomposite decreases from 7.5×10^{-23} (m^2.m/m^2.s.Pa) up to 4.3×10^{-24} (m^3.m/m^2.s.Pa) by only adding 40% of VMT to CS in dry conditions, also the oxygen permeability of two layers of nanocomposite can reach a value lower than 2.3×10^{-24} (m^3.m/m^2.s.Pa) for 50 wt.% VMT. Even if higher effect on the gas barrier properties could be expected, however, the limit of detection of the apparatus is attained and the evolution cannot be detected as seen in Fig. 8b. We can conclude that the presence of clay nanoparticles in a CS matrix changes the permeation mechanisms by increasing the effective path length for diffusion when a permeant goes through the material from one surface to another.

4. Conclusions

In this study, the corona treatment of PET films for water-based coatings has been optimized. Exfoliated CS-VMT nanocomposites can be prepared by simple mixing of acid modified VMT solution with acidified aqueous solution of CS followed by bar-coating process. Thickness of the coated layers was successfully determined by SEM (from 1 to 4 μm). Helium and oxygen permeance of PET films coated with CS were measured with a drop of two decades compared to PET. After adding the VMT to the CS the helium and oxygen permeances decrease when the composition of the nanocomposite increased on VMT. BiF about 100 in helium and more than 10 in oxygen were obtained when adding 50% of VMT which make those coatings more efficient than PVDC ones in dry conditions.

Acknowledgements

The work was supported by the Islamic Development Bank of the kingdom of Saudi Arabia with the PhD funding (grant number 3611209368).

We thank Christophe Poulard, from the Laboratoire des Physique des solides (LPS, France) for assistance with contact angle measurements, Catherine Gomez from molecular chemistry laboratory and the engineering of chemical and energy processes (CMGPCE, Cnam, France) for DLS measurements and discussions, Sophie Norvez from Laboratory of Matière Molle et Chime (ESPCI, France) for assistance with Transmission electron microscopy analysis, doctor Thomas Karbowiack and professor Frédéric Debeaufort at the University of Bourgogne for comments that greatly improved the manuscript.

References

Abugoch, L. E., Tapia, C., Villamán, M. C., Yazdani-Pedram, M., & Díaz-Dosque, M. (2011). Characterization of quinoa protein–chitosan blend edible films. *Food Hydrocolloids, 25*(5), 879–886. https://doi.org/10.1016/j.foodhyd.2010.08.008.

Azeez, A. A., Rhee, K. Y., Park, S. J., & Hui, D. (2013). Epoxy clay nanocomposites – Processing, properties and applications: A review. *Composites Part B Engineering, 45*(1), 308–320. https://doi.org/10.1016/j.compositesb.2012.04.012.

Benbettaïeb, N., Assifaoui, A., Karbowiak, T., Debeaufort, F., & Chambin, O. (2016). Controlled release of tyrosol and ferulic acid encapsulated in chitosan–gelatin films after electron beam irradiation. *Radiation Physics and Chemistry, 118*, 81–86. https://doi.org/10.1016/j.radphyschem.2015.01.035.

Benbettaïeb, N., Karbowiak, T., Bornaz, S., & Debeaufort, F. (2015). Spectroscopic analyses of the influence of electron beam irradiation doses on mechanical, transport properties and microstructure of chitosan-fish gelatin blend films. *Food Hydrocolloids, 46*, 37–51. https://doi.org/10.1016/j.foodhyd.2014.09.038.

Benbettaïeb, N., Karbowiak, T., Brachais, C.-H., & Debeaufort, F. (2015). Coupling tyrosol, quercetin or ferulic acid and electron beam irradiation to cross-link chitosan–gelatin films: A structure–Function approach. *European Polymer Journal, 67*, 113–127. https://doi.org/10.1016/j.eurpolymj.2015.03.060.

Berne, B. J., & Pecora, R. (2000). *Dynamic light scattering: With applications to chemistry, biology, and physics.* Courier Corporation.

Bhaskar, T., Tanabe, M., Muto, A., & Sakata, Y. (2006). Pyrolysis study of a PVDC and HIPS-Br containing mixed waste plastic stream: Effect of the poly(ethylene terephthalate). *Journal of Analytical and Applied Pyrolysis, 77*(1), 68–74. https://doi.org/10.1016/j.jaap.2006.01.005.

Bordes, P., Pollet, E., & Avérous, L. (2009). Nano-biocomposites: Biodegradable polyester/nanoclay systems. *Progress in Polymer Science, 34*(2), 125–155. https://doi.org/10.1016/j.progpolymsci.2008.10.002.

Bourtoom, T. (2008). Edible films and coatings: Characteristics and properties. *International Food Research Journal, 15*(3), 237–248.

Caner, C., Vergano, P. J., & Wiles, J. L. (1998). Chitosan film mechanical and permeation properties as affected by acid, plasticizer, and storage. *Journal of Food Science, 63*(6), 1049–1053. https://doi.org/10.1111/j.1365-2621.1998.tb15852.x.

Casariego, A., Souza, B. W. S., Cerqueira, M. A., Teixeira, J. A., Cruz, L., Díaz, R., … Vicente, A. A. (2009). Chitosan/clay films' properties as affected by biopolymer and clay micro/nanoparticles' concentrations. *Food Hydrocolloids, 23*(7), 1895–1902. https://doi.org/10.1016/j.foodhyd.2009.02.007.

Chung, Y.-L., Ansari, S., Estevez, L., Hayrapetyan, S., Giannelis, E. P., & Lai, H.-M. (2010). Preparation and properties of biodegradable starch–clay nanocomposites. *Carbohydrate Polymers, 79*(2), 391–396. https://doi.org/10.1016/j.carbpol.2009.08.021.

Cussler, E. L., Hughes, S. E., Ward, W. J., & Aris, R. (1988). Barrier membranes. *Journal of Membrane Science, 38*(2), 161–174. https://doi.org/10.1016/S0376-7388(00)80877-7.

David, G., & Pérez, J. (2009). Combined sampler robot and high-performance liquid chromatography: A fully automated system for biological small-angle X-ray scattering experiments at the synchrotron SOLEIL SWING beamline. *Journal of Applied Crystallography, 42*(5), 892–900. https://doi.org/10.1107/S0021889809029288.

de Azeredo, H. M. C. (2009). Nanocomposites for food packaging applications. *Food Research International, 42*(9), 1240–1253. https://doi.org/10.1016/j.foodres.2009.03.019.

Dehghani, S., Hosseini, S. V., & Regenstein, J. M. (2018). Edible films and coatings in seafood preservation: A review. *Food Chemistry, 240*(Supplement C), 505–513. https://doi.org/10.1016/j.foodchem.2017.07.034.

Duncan, T. V. (2011). Applications of nanotechnology in food packaging and food safety: Barrier materials, antimicrobials and sensors. *Journal of Colloid and Interface Science, 363*(1), 1–24. https://doi.org/10.1016/j.jcis.2011.07.017.

Elsabee, M. Z., & Abdou, E. S. (2013). Chitosan based edible films and coatings: A review. *Materials Science and Engineering C, 33*(4), 1819–1841. https://doi.org/10.1016/j.msec.2013.01.010.

Epure, V., Griffon, M., Pollet, E., & Avérous, L. (2011). Structure and properties of glycerol-plasticized chitosan obtained by mechanical kneading. *Carbohydrate Polymers, 83*(2), 947–952. https://doi.org/10.1016/j.carbpol.2010.09.003.

Fajardo, P., Martins, J. T., Fuciños, C., Pastrana, L., Teixeira, J. A., & Vicente, A. A. (2010). Evaluation of a chitosan-based edible film as carrier of natamycin to improve the storability of Saloio cheese. *Journal of Food Engineering, 101*(4), 349–356. https://doi.org/10.1016/j.jfoodeng.2010.06.029.

Fowkes, F. M. (1964). Attractive forces at interfaces. *Industrial and Engineering Chemistry, 56*(12), 40–52. https://doi.org/10.1021/ie50660a008.

Giannakas, A., Spanos, C. G., Kourkoumelis, N., Vaimakis, T., & Ladavos, A. (2008). Preparation, characterization and water barrier properties of PS/organo-montmorillonite nanocomposites. *European Polymer Journal, 44*(12), 3915–3921. https://doi.org/10.1016/j.eurpolymj.2008.10.001.

Gorrasi, G., Pantani, R., Murariu, M., & Dubois, P. (n.d.). PLA/Halloysite Nanocomposite Films: Water Vapor Barrier Properties and Specific Key Characteristics. Macromolecular Materials and Engineering, 299(1), 104–115. https://doi.org/https://doi.org/10.1002/mame.201200424.

Han, S.-H., Kim, B.-J., & Park, J.-S. (2014). Effects of the corona pretreatment of PET substrates on the properties of flexible transparent CNT electrodes. *Thin Solid Films, 572*, 73–78. https://doi.org/10.1016/j.tsf.2014.09.066.

Haworth, B., & Robinson, T. M. (1991). The measurement of thin PVdC coatings on PET substrates using fluorescence microscopy. *Polymer Testing, 10*(3), 205–219. https://doi.org/10.1016/0142-9418(91)90033-T.

Kurek, M., Brachais, C.-H., Ščetar, M., Voilley, A., Galić, K., Couvercelle, J.-P., … Debeaufort, F. (2013). Carvacrol affects interfacial, structural and transfer properties of chitosan coatings applied onto polyethylene. *Carbohydrate Polymers, 97*(1), 217–225. https://doi.org/10.1016/j.carbpol.2013.04.059.

Kurek, M., Ščetar, M., Voilley, A., Galić, K., & Debeaufort, F. (2012). Barrier properties of chitosan coated polyethylene. *Journal of Membrane Science, 403–404*, 162–168. https://doi.org/10.1016/j.memsci.2012.02.037.

Kurek, M., Galus, S., & Debeaufort, F. (2014). Surface, mechanical and barrier properties of bio-based composite films based on chitosan and whey protein. *Food Packaging and Shelf Life, 1*(1), 56–67. https://doi.org/10.1016/j.fpsl.2014.01.001.

Kurek, M., Guinault, A., Voilley, A., Galić, K., & Debeaufort, F. (2014). Effect of relative humidity on carvacrol release and permeation properties of chitosan based films and coatings. *Food Chemistry, 144*, 9–17. https://doi.org/10.1016/j.foodchem.2012.11.132.

Laufer, G., Kirkland, C., Cain, A. A., & Grunlan, J. C. (2013). Oxygen barrier of multilayer thin films comprised of polysaccharides and clay. *Carbohydrate Polymers, 95*(1), 299–302. https://doi.org/10.1016/j.carbpol.2013.02.048.

Lertsutthiwong, P., Noomun, K., Khunthon, S., & Limpanart, S. (2012). Influence of chitosan characteristics on the properties of biopolymeric chitosan–montmorillonite. *Progress in Natural Science: Materials International, 22*(5), 502–508. https://doi.org/10.1016/j.pnsc.2012.07.008.

Lewandowska, K., Sionkowska, A., Kaczmarek, B., & Furtos, G. (2014). Characterization of chitosan composites with various clays. *International Journal of Biological Macromolecules, 65*, 534–541. https://doi.org/10.1016/j.ijbiomac.2014.01.069.

Liu, G., Zhan, J., Zheng, M., Li, L., Li, C., Jiang, X., … Jin, R. (2015). Field pilot study on emissions, formations and distributions of PCDD/Fs from cement kiln co-processing fly ash from municipal solid waste incinerations. *Journal of Hazardous Materials, 299*, 471–478. https://doi.org/10.1016/j.jhazmat.2015.07.052.

Madeleine-Perdrillat, C., Karbowiak, T., Raya, J., Gougeon, R., Bodart, P. R., & Debeaufort, F. (2015). Water-induced local ordering of chitosan polymer chains in thin layer films. *Carbohydrate Polymers, 118*, 107–114. https://doi.org/10.1016/j.carbpol.2014.11.001.

O'Hare, L.-A., Smith, J. A., Leadley, S. R., Parbhoo, B., Goodwin, A. J., & Watts, J. F. (2002). Surface physico-chemistry of corona-discharge-treated poly(ethylene terephthalate) film. *Surface and Interface Analysis, 33*(7), 617–625. https://doi.org/10.1002/sia.1429.

Ohta, M., Oshima, S., Iwasa, T., Osawa, N., Kumatoriya, K., Yamazaki, A., … Umedzu, N. (2001). Formation of PCDDs and PCDFs during the combustion of polyvinylidene chloride. *Chemosphere, 44*(6), 1389–1394. https://doi.org/10.1016/S0045-6535(00)00540-3.

Ohta, M., Oshima, S., Osawa, N., Iwasa, T., & Nakamura, T. (2004). Formation of PCDDs and PCDFs during the combustion of polyvinylidene chloride and other polymers in the presence of HCl. *Chemosphere, 54*(10), 1521–1531. https://doi.org/10.1016/j.chemosphere.2003.07.002.

Owens, D. K., & Wendt, R. C. (2003). Estimation of the surface free energy of polymers. *Journal of Applied Polymer Science, 13*(8), 1741–1747. https://doi.org/10.1002/app.1969.070130815.

Park, S.-J., & Jin, J.-S. (2001). Effect of corona discharge treatment on the dyeability of low-density polyethylene film. *Journal of Colloid and Interface Science, 236*(1), 155–160. https://doi.org/10.1006/jcis.2000.7380.

Pavlidou, S., & Papaspyrides, C. D. (2008). A review on polymer–layered silicate nanocomposites. *Progress in Polymer Science, 33*(12), 1119–1198. https://doi.org/10.1016/j.progpolymsci.2008.07.008.

Petrova, V. A., Nud'ga, L. A., Bochek, A. M., Yudin, V. E., Gofman, I. V., Elokhovskii, V. Y., … Dobrovol'skaya, I. P. (2012). Specific features of chitosan-montmorillonite interaction in an aqueous acid solution and properties of related composite films. *Polymer Science Series A, 54*(3), 224–230. https://doi.org/10.1134/S0965545X1203008X.

Picard, E., Vermogen, A., Gérard, J.-F., & Espuche, E. (2007). Barrier properties of nylon 6-montmorillonite nanocomposite membranes prepared by melt blending: Influence of the clay content and dispersion state: Consequences on modelling. *Journal of Membrane Science, 292*(1), 133–144. https://doi.org/10.1016/j.memsci.2007.01.030.

Pochan, J. M., Gerenser, L. J., & Elman, J. F. (1986). An e.s.c.a. study of the gas-phase derivatization of poly(ethylene terephthalate) treated by dry-air and dry-nitrogen corona discharge. *Polymer, 27*(7), 1058–1062. https://doi.org/10.1016/0032-3861(86)90072-8.

Ray, S. S., & Bousmina, M. (2005). Biodegradable polymers and their layered silicate nanocomposites: In greening the 21st century materials world. *Progress in Materials*

Science, 50(8), 962–1079. https://doi.org/10.1016/j.pmatsci.2005.05.002.
Reis, A. B., Yoshida, C. M., Reis, A. P. C., & Franco, T. T. (2011). Application of chitosan emulsion as a coating on Kraft paper. *Polymer International, 60*(6), 963–969. https://doi.org/10.1002/pi.3023.
Ren, L., Yan, X., Zhou, J., Tong, J., & Su, X. (2017). Influence of chitosan concentration on mechanical and barrier properties of corn starch/chitosan films. *International Journal of Biological Macromolecules, 105*, 1636–1643. https://doi.org/10.1016/j.ijbiomac.2017.02.008.
Rhim, J.-W. (2011). Effect of clay contents on mechanical and water vapor barrier properties of agar-based nanocomposite films. *Carbohydrate Polymers, 86*(2), 691–699. https://doi.org/10.1016/j.carbpol.2011.05.010.
Rhim, J. W., Gennadios, A., Weller, C. L., & Hanna, M. A. (2002). Sodium dodecyl sulfate treatment improves properties of cast films from soy protein isolate. *Industrial Crops and Products, 15*(3), 199–205. https://doi.org/10.1016/S0926-6690(01)00114-5.
Rhim, J.-W., Park, H.-M., & Ha, C.-S. (2013). Bio-nanocomposites for food packaging applications. *Progress in Polymer Science, 38*(10), 1629–1652. https://doi.org/10.1016/j.progpolymsci.2013.05.008.
Rocca-Smith, J. R., Karbowiak, T., Marcuzzo, E., Sensidoni, A., Piasente, F., Champion, D., ... Debeaufort, F. (2016). Impact of corona treatment on PLA film properties. *Polymer Degradation and Stability, 132*, 109–116. https://doi.org/10.1016/j.polymdegradstab.2016.03.020.
Roilo, D., Maestri, C. A., Scarpa, M., Bettotti, P., & Checchetto, R. (2018). Gas barrier and optical properties of cellulose nanofiber coatings with dispersed TiO2 nanoparticles. *Surface & Coatings Technology, 343*, 131–137. https://doi.org/10.1016/j.surfcoat.2017.10.015.
Sánchez-González, L., Cháfer, M., Chiralt, A., & González-Martínez, C. (2010). Physical properties of edible chitosan films containing bergamot essential oil and their inhibitory action on Penicillium italicum. *Carbohydrate Polymers, 82*(2), 277–283. https://doi.org/10.1016/j.carbpol.2010.04.047.
Sathivel, S., Liu, Q., Huang, J., & Prinyawiwatkul, W. (2007). The influence of chitosan glazing on the quality of skinless pink salmon (Oncorhynchus gorbuscha) fillets during frozen storage. *Journal of Food Engineering, 83*(3), 366–373. https://doi.org/10.1016/j.jfoodeng.2007.03.009.
Shahidi, F., Arachchi, J. K. V., & Jeon, Y.-J. (1999). Food applications of chitin and chitosans. *Trends in Food Science & Technology, 10*(2), 37–51. https://doi.org/10.1016/S0924-2244(99)00017-5.
Shenton, M. J., & Stevens, G. C. (2001). Surface modification of polymer surfaces: Atmospheric plasma versus vacuum plasma treatments. *Journal of Physics D: Applied Physics, 34*(18), 2761. https://doi.org/10.1088/0022-3727/34/18/308.
Sinha Ray, S., & Okamoto, M. (2003). Polymer/layered silicate nanocomposites: A review from preparation to processing. *Progress in Polymer Science, 28*(11), 1539–1641. https://doi.org/10.1016/j.progpolymsci.2003.08.002.
Ström, G., Fredriksson, M., & Stenius, P. (1987). Contact angles, work of adhesion, and interfacial tensions at a dissolving Hydrocarbon surface. *Journal of Colloid and Interface Science, 119*(2), 352–361. https://doi.org/10.1016/0021-9797(87)90280-3.
Sutherland, I., Popat, R. P., Brewis, D. M., & Calder, R. (1994). Corona discharge treatment of polyolefins. *The Journal of Adhesion, 46*(1–4), 79–88. https://doi.org/10.1080/00218469408026651.
Takahashi, S., Goldberg, H. A., Feeney, C. A., Karim, D. P., Farrell, M., O'Leary, K., ... Paul, D. R. (2006). Gas barrier properties of butyl rubber/vermiculite nanocomposite coatings. *Polymer, 47*(9), 3083–3093. https://doi.org/10.1016/j.polymer.2006.02.077.
Tang, C., Chen, N., Zhang, Q., Wang, K., Fu, Q., & Zhang, X. (2009). Preparation and properties of chitosan nanocomposites with nanofillers of different dimensions. *Polymer Degradation and Stability, 94*(1), 124–131. https://doi.org/10.1016/j.polymdegradstab.2008.09.008.
Tharanathan, R. N. (2003). Biodegradable films and composite coatings: Past, present and future. *Trends in Food Science & Technology, 14*(3), 71–78. https://doi.org/10.1016/S0924-2244(02)00280-7.
Tortora, M., Gorrasi, G., Vittoria, V., Galli, G., Ritrovati, S., & Chiellini, E. (2002). Structural characterization and transport properties of organically modified montmorillonite/polyurethane nanocomposites. *Polymer, 43*(23), 6147–6157. https://doi.org/10.1016/S0032-3861(02)00556-6.
Tsay, C.-Y., & Pai, K.-C. (2018). Properties of Al-Ga co-doped ZnO semiconductor thin films deposited on polyethylene terephthalate substrates by radio frequency magnetron sputtering. *Thin Solid Films, 654*, 11–15. https://doi.org/10.1016/j.tsf.2018.03.077.
Wang, S., & Jing, Y. (2017). Effects of formation and penetration properties of biodegradable montmorillonite/chitosan nanocomposite film on the barrier of package paper. *Applied Clay Science, 138*, 74–80. https://doi.org/10.1016/j.clay.2016.12.037.
Wang, S. F., Shen, L., Tong, Y. J., Chen, L., Phang, I. Y., Lim, P. Q., ... Liu, T. X. (2005). Biopolymer chitosan/montmorillonite nanocomposites: Preparation and characterization. *Polymer Degradation and Stability, 90*(1), 123–131. https://doi.org/10.1016/j.polymdegradstab.2005.03.001.
Wang, S.-F., Shen, L., Zhang, W.-D., & Tong, Y.-J. (2005). Preparation and mechanical properties of chitosan/carbon nanotubes composites. *Biomacromolecules, 6*(6), 3067–3072. https://doi.org/10.1021/bm050378v.
Wikström, F., Williams, H., & Venkatesh, G. (2016). The influence of packaging attributes on recycling and food waste behavior—An environmental comparison of two packaging alternatives. *Journal of Cleaner Production, 137*, 895–902. https://doi.org/10.1016/j.jclepro.2016.07.097.
Xu, Y., Ren, X., & Hanna, M. A. (2006). Chitosan/clay nanocomposite film preparation and characterization. *Journal of Applied Polymer Science, 99*(4), 1684–1691. https://doi.org/10.1002/app.22664.
Yixiang, X., Xi, R., & & A, H. M. (2006). Chitosan/clay nanocomposite film preparation and characterization. *Journal of Applied Polymer Science, 99*(4), 1684–1691. https://doi.org/10.1002/app.22664.
Yu, Q., Song, Y., Shi, X., Xu, C., & Bin, Y. (2011). Preparation and properties of chitosan derivative/poly(vinyl alcohol) blend film crosslinked with glutaraldehyde. *Carbohydrate Polymers, 84*(1), 465–470. https://doi.org/10.1016/j.carbpol.2010.12.006.